Chemical exchange saturation transfer imaging in hepatic encephalopathy

Helge Jörn Zöllner[a,b,]*, Markus Butz[a], Markus Jördens[c], Nur-Deniz Füllenbach[c], Dieter Häussinger[c], Benjamin Schmitt[d], Hans-Jörg Wittsack[b], Alfons Schnitzler[a]

[a] Institute of Clinical Neuroscience and Medical Psychology, Medical Faculty, Heinrich Heine University Düsseldorf, Germany
[b] Department of Diagnostic and Interventional Radiology, Medical Faculty, Heinrich Heine University Düsseldorf, Germany
[c] Department of Gastroenterology, Hepatology and Infectiology, Medical Faculty, Heinrich Heine University Düsseldorf, Germany
[d] Siemens Ltd. Australia, Healthcare Sector, 160 Herring Road, Macquarie Park, NSW 2113, Australia

ARTICLE INFO

ABSTRACT

Hepatic encephalopathy (HE) is a common complication in liver cirrhosis and associated with an invasion of ammonia into the brain through the blood-brain barrier. Resulting higher ammonia concentrations in the brain are suggested to lead to a dose-dependent gradual increase of HE severity and an associated impairment of brain function. Amide proton transfer-weighted (APT_w) chemical exchange saturation transfer (CEST) imaging has been found to be sensitive to ammonia concentration. The aim of this work was to study APT_w CEST imaging in patients with HE and to investigate the relationship between disease severity, critical flicker frequency (CFF), psychometric test scores, blood ammonia, and APT_w signals in different brain regions.

Whole-brain APT_w CEST images were acquired in 34 participants (14 controls, 20 patients (10 minimal HE, 10 manifest HE)) on a 3 T clinical MRI system accompanied by T_1 mapping and structural images. T_1 normalized magnetization transfer ratio asymmetry analysis was performed around 3 ppm after B_0 and B_1 correction to create APT_w images. All APT_w images were spatially normalized into a cohort space to allow direct comparison. APT_w images in 6 brain regions (cerebellum, occipital cortex, putamen, thalamus, caudate, white matter) were tested for group differences as well as the link to CFF, psychometric test scores, and blood ammonia.

A decrease in APT_w intensities was found in the cerebellum and the occipital cortex of manifest HE patients. In addition, APT_w intensities in the cerebellum correlated positively with several psychometric scores, such as the fine motor performance scores MLS1 for hand steadiness / tremor ($r = 0.466$; $p = .044$) and WRT2 for motor reaction time ($r = 0.523$; $p = .022$). Moreover, a negative correlation between APT_w intensities and blood ammonia was found for the cerebellum ($r = -0.615$; $p = .007$) and the occipital cortex ($r = -0.478$; $p = .045$). An increase of APT_w intensities was observed in the putamen of patients with minimal HE and correlated negatively with the CFF ($r = -0.423$; $p = .013$).

Our findings demonstrate that HE is associated with regional differential alterations in APT_w signals. These variations are most likely a consequence of hyperammonemia or hepatocerebral degeneration processes, and develop in parallel with disease severity.

1. Introduction

Liver cirrhosis is known to manifest in systemic effects. In particular, the most common neurological manifestation of liver cirrhosis is hepatic encephalopathy (HE), which comprises a variety of symptoms. Patients suffering from HE exhibit alterations in cognitive and motor function as well as behavioral changes. The clinical symptoms of HE vary with disease severity, starting with mild attentional deficits and disorientation, cognitive deterioration, and disturbed motor control. They may develop into somnolence and stupor and in the most severe case hepatic coma (Butterworth, 2000; Felipo, 2013; Ferenci et al., 2002; Prakash and Mullen, 2010).

The pathophysiology of HE is not finally understood, but is assumed to be multifactorial (Cichoz-Lach and Michalak, 2013; Felipo, 2013;

Häussinger and Sies, 2013). A key element in the pathophysiology is the invasion of ammonia into the brain through the blood-brain barrier. Previous studies using $^{13}NH_3$-PET imaging have revealed an increased uptake of circulating ammonia into the brain of cirrhosis patients (Keiding et al., 2006; Lockwood et al., 1991).

In addition to increased oxidative stress caused by ammonia accumulation (Norenberg et al., 2005), an excess of glutamine is produced in the astrocytes as a result of ammonia detoxification by glutamine synthetase. The increased glutamine concentration in the astrocytes triggers cell swelling *via* osmotic imbalance, finally leading to alteration of brain water homeostasis and emergence of a low-grade edema (Detry et al., 2006; Häussinger and Schliess, 2008). The emergence of a low-grade edema was further investigated by different studies using advanced MR imaging: Quantitative T_1 mapping and semi-solid magnetization transfer (MTC) imaging studies attributed increased T_1 values (Shah et al., 2003) and alterations in the calculated MTC effect (Miese et al., 2006) to increased water content in HE patients. Additionally, a quantitative water mapping approach has demonstrated a small increase of water content in white matter areas (Shah et al., 2008), while these findings remained absent in another quantitative water mapping study including patients with low-grade HE (Oeltzschner et al., 2016). In general, T_1-weighted (Butterworth et al., 1995; Klos et al., 2006; Pujol et al., 1993; Rovira et al., 2008) or quantitative T_1 (Shah et al., 2003) imaging may be altered by increased water content. However, T_1 changes especially within the basal ganglia are more likely to be mediated by manganese deposition, which is a common neurotoxin in HE (Rose et al., 1999).

All MR visible effects described above are based on the notion of ammonia accumulation in the patients' brains. Therefore, it is of paramount interest to measure ammonia in a most direct way, without the use of radiation, and with increased resolution compared to $^{13}NH_3$-PET imaging.

Chemical exchange saturation transfer (CEST) represents a suitable tool for the assessment of changes of *in vivo* ammonia levels. CEST provides an advanced MRI contrast depending on diluted labile protons, which are usually undetectable by conventional MRI. The CEST contrast is based on the mitigation of the bulk water signal due to magnetization transfer between the bulk water and frequency-selectively saturated labile protons (Wolff and Balaban, 1989). Amide proton transfer-weighted (APT_w) imaging, which is based on magnetization transfer from exchangeable amide protons of mobile tissue proteins and peptides (Jones et al., 2012), is an emerging field in CEST imaging. It allows several applications, such as amide proton quantification, detection of pH changes in the amide proton environment (Mori et al., 1998; van Zijl et al., 2003; Zhou et al., 2003a), and measurement of global *in vitro* protein folding (Goerke et al., 2017, 2015) with possible applications in neurodegenerative diseases. Additionally, CEST depends on non-exchange-related factors, such as direct water saturation, MTC, and water longitudinal relaxation time (Zu, 2018). Thus, these factors have to be included in the interpretation of possible HE related changes in APT_w imaging.

In our recent *in vitro* study, we were able to link increasing ammonia concentrations to a decreasing APT_w CEST signal through protein denaturation (Zöllner et al., 2018). We could also apply this finding to example cases of HE patients. The present study aimed to systematically investigate the sensitivity of APT_w imaging to HE-related brain ammonia levels, and to gauge its potential to monitor disease severity and progression *via* the HE-related signal alteration in APT_w imaging. To this end, APT_w imaging was performed in a cohort of clinically well-characterized HE patients in different grades of severity, as well as healthy age-matched controls. To investigate the relationship between disease severity and APT_w imaging, the critical flicker frequency (CFF), psychometric testing scores, and blood ammonia levels were assessed. In addition, T_1 maps were acquired to control for T_1 effects on the measured MTR_{asym} values by T_1 normalization in the region-of-interest analysis.

2. Material and methods

2.1. Participants and HE grading

The study was performed in accordance with the Declaration of Helsinki in its current version ("*World Medical Association declaration of Helsinki: Ethical principles for medical research involving human subjects*", 2013), and was approved by the local institutional review board (study number 5179R). All participants gave written informed consent prior to the examination. 15 controls and 20 patients with clinically confirmed HE, graded as minimal HE (mHE) and manifest HE (HE), were examined. Exclusion criteria for both patients and controls included neurological or psychiatric diseases excluding the diagnosis of HE for the patient group, severe intestinal diseases, the use of any medication acting on the central nervous system and diagnosed peripheral/retinal neuropathy. If alcohol abuse was part of the medical history, the patient had to remain abstinent for ≥ 4 weeks prior to examination. The grading was performed in line with the *West-Haven* criteria (Ferenci et al., 2002; Kircheis et al., 2002). In addition, neuropsychological testing, critical flicker frequency (CFF) assessment with portable CFF goggles (NEVOlab, Maierhöfen, Germany), and blood sample tests were carried out. In the CFF test, the tested individual has to indicate with a button press when the impression of a virtual light source in 12 m distance changes from a fused light source to a flickering one. After a short training session, the CFF is assessed eight times, and the mean and standard deviation are calculated for further analysis. The CFF was included as it has been shown to be a reliable clinical parameter for HE monitoring, and accounts for the continuous nature of symptom severity (Kircheis et al., 2014, 2002). One control had to be excluded due to a CFF value < 39 Hz, which is the cut-off frequency for mHE. The remaining study population is summarized in Table 1.

HE severity was determined by an experienced clinician and included a clinical assessment regarding the mental state and consciousness of the patients and neuropsychometric testing. Computer-based neuropsychometric tests from the Vienna Test System (Dr. Schuhfried GmbH, Mödling, Austria) consisted of five test batteries and reported 22 age-validated scores (percentile rank values in comparison to an age-matched control cohort) reflecting motor and cognitive performance. Better performance was graded with higher scores. The parameter values were considered as abnormal in case of a percentile rank lower than 15.9 compared to the control cohort implemented in the test system. Patients without clinical symptoms of manifest HE, but with > 1 abnormal psychometric test result were classified as mHE (Kircheis et al., 2002). Selected scores were incorporated for further analysis, including cognitive (COG1: time to reject a geometric shape not matching control shapes; COG2: time to confirm a geometric shape matching a control shape), fine motor performance (line following test: LVT1: time per item; LVT2: overall score), motor/precision/speed (MLS1: hand steadiness/tremor; MLS2: arm/hand precision; MLS3: arm/hand speed; MLS4: finger tapping speed), and reaction

Table 1
Remaining study cohort.

	N	Sex [M/F]	Age [years] Mean ± SD	CFF [Hz] Mean ± SD	Etiology of liver cirrhosis
Controls	14	8/6	60.1 ± 5.3	44.2 ± 3.4	–
mHE	10	7/3	55.1 ± 10.4	41.0 ± 3.2*	5 ALC, 1 HCV, 1 NASH, 1 OS, 2 U
HE	10	6/4	59.5 ± 6.7	36.4 ± 2.3**	5 ALC, 2 HCV, 2 NASH, 1 OS

* Significantly different from controls ($p < .05$) with non-parametric Wilcoxon rank sum test.

** Significantly different from controls ($p < .01$) and mHE ($p < .01$) with non-parametric Wilcoxon rank sum test (*ALC* alcoholic, *HCV* hepatitis C virus, *NASH* non-alcoholic steatohepatitis, *OS* overlap syndrome, *U* unknown).

Table 2
Atlas based statistics of APT_w^{T1} MTR_{asym} in HE (minimal HE (mHE), manifest HE (HE)).

	T_1 normalized MTR_{asym} (%) Mean (± SD)			Correlation with		
	Control	Patients		CFF	Blood ammonia	GGT
		mHE	HE	r p	r p	r p
Cerebellum	0.94 (0.48)	0.92 (1.16)	**0.61**[#] **(0.75)**	0.043 0.807	**−0.615** **0.007**	−0.251 0.300
Occipital cortex	0.82 (0.60)	0.88 (0.50)	**0.39*** **(0.50)**	0.102 0.564	**−0.478** **0.045**	−0.267 0.269
Putamen	0.61 (0.11)	**0.76*** **(0.09)**	0.81 (0.24)	**−0.423** **0.013**	−0.285 0.252	−0.393 0.096
Thalamus	0.43 (0.08)	0.45 (0.08)	0.48 (0.18)	−0.323 0.062	−0.365 0.137	**−0.454** **0.049**
Caudate	0.35 (0.12)	0.37 (0.13)	0.42 (0.16)	−0.200 0.257	−0.221 0.379	−0.008 0.975
White matter	0.49 (0.08)	0.51 (0.12)	0.57 (0.14)	−0.231 0.190	−0.409 0.137	−0.048 0.847

Asterisks indicate significant differences from controls (* = $p < .05$). Pound signs indicate significant differences between patient groups ([#] = p < .05). Bold numbers indicate significant correlations over all participants. Reduced APT_w^{T1} MTR_{asym} and its correlation with blood ammonia in cerebellar and occipital regions indicate either increased ammonia accumulation or hepatocerebral degeneration. Increased putaminal APT_w^{T1} MTR_{asym} are related to other contrast mechanisms, such as strong alterations in metabolite concentrations.

for $p < .05$.

Relationships between CFF and APT_w^{T1} MTR_{asym}, blood ammonia and APT_w^{T1} MTR_{asym}, and between psychometric scores and APT_w^{T1} MTR_{asym} were compared with a bivariate two-sided Pearson correlation test. Correlations were considered significant in case $p < .05$. No multiple comparison correction was employed in the analysis.

All statistical analyses were performed using IBM SPSS Statistics for Windows, Version 24.0 (IBM Corp., Armonk, NY, USA).

3. Results

All 34 MRI datasets (14 controls, 10 mHE, 10 HE) remained in the final analysis. The manifest HE group included 9 HE I patients and one patient graded as HE II. One HE I patient did not undergo psychometric testing, and two patients did not undergo blood testing (1 mHE, 1 HE).

3.1. APT_w atlases

Mean group APT_w atlases are depicted in Fig. 1. The atlases indicate decreasing APT_w MTR_{asym} in the cerebellum and the occipital region of the manifest HE patients. In addition, slight alterations in deep grey matter regions are occurring, as APT_w MTR_{asym} increases within the Putamen. An absence of changes is visible for caudate, thalamus, and the selected white matter region.

Supplementary Fig. 1 represents the mean APT_w atlases, as well as the corresponding slices of mean T1 atlases. To avoid any contamination of APT_w effects by water longitudinal relaxation, a T_1 normalization was performed in the ROI based analysis. Group results and correlations with critical flicker frequency (CFF), blood ammonia, and gamma-glutamyltransferase (GGT) concentration are summarized in Table 2. The ROI based analysis is summarized in the following sections. The figures are focused on the ROI with significant differences in the measured APT_w^{T1} MTR_{asym}.

3.2. Cerebellum

Mean cerebellar APT_w^{T1} MTR_{asym} values were reduced in HE patients compared to mHE patients ($p < .05$; Fig. 2a) indicating higher levels of ammonia or hepatocerebral degeneration in the patients with manifest HE compared to minimal HE. No differences were found between controls compared to both patient groups. A negative correlation of cerebellar APT_w imaging blood ammonia levels ($r = −0.615$; $p = .013$; Fig. 2b) and a positive correlation with the psychometric MLS1 (hand steadiness / tremor) score ($r = 0.466$; $p = .044$; Fig. 2c) were found. Furthermore, a positive correlation of the psychometric WRT2 score and mean APT_w^{T1} MTR_{asym} could be observed ($r = 0.523$; $p = .022$; Fig. 2d).

3.3. Occipital cortex

A decrease in mean APT_w^{T1} MTR_{asym} was observed between controls and HE patients ($p < .05$), whereas no significant differences were detected between controls and mHE patients and between both patient groups (Fig. 3a). A negative correlation of occipital APT_w imaging and blood ammonia levels ($r = −0.476$; $p = .045$; Fig. 3b) and a positive correlation with the psychometric MLS2 (arm/hand precision) score ($r = 0.544$; $p = .016$; Fig. 3c) were present. A positive correlation of occipital APT_w imaging and psychometric MLS2 (arm/hand precision) score ($r = 0.544$; $p = .016$; Fig. 3c) and a negative correlation with blood ammonia levels ($r = −0.476$; $p = .045$; Fig. 3b) were present. Additionally, a positive correlation between the psychometric LVT1 score and the mean APT_w^{T1} MTR_{asym} was found (Fig. 3d).

3.4. Putamen

Mean putaminal APT_w^{T1} MTR_{asym} were increased in mHE patients compared to controls ($p < .05$), whereas no differences were found between controls and HE patients and between the two patient groups (Fig. 4a). Additionally, the mean values in the HE patient group showed a greater variability. A negative correlation of CFF and APT_w^{T1} MTR_{asym} was observed (Fig. 4b). In contrast to the cerebellar and occipital region, the increased putaminal APT_w^{T1} MTR_{asym} suggests the domination of other contrast mechanism, such as increased glutamine concentrations, in this region. Alterations through increased water or the accumulation of manganese were ruled out by T_1 normalization.

3.5. Psychometric testing

Results of the correlation analysis of the psychometric tests are summarized in Table 3. The motor score MLS and the motor reaction time score WRT2 correlated positively with the APT_w^{T1} intensities in the cerebellum. This indicates a connection between motor deficits of HE patients and reduced APT_w^{T1} MTR_{asym} in the cerebellum. The line following scores LVT1 and LVT2, the motor scores MLS2 and MLS3, as well as the motor reaction time WRT2 correlated positively with the observed APT_w^{T1} intensities in the occipital cortex.

4. Discussion

In the present *in vivo* CEST study, we applied chemical exchange saturation transfer imaging to investigate the link between hepatic encephalopathy, blood ammonia levels, and APT_w measures which reflect cerebral ammonia levels. Our results reveal reduced APT_w^{T1} MTR_{asym} within the cerebellum and occipital regions correlating both with blood ammonia and psychometric scores. Additionally, APT_w intensities are increased within the putamen of mHE patients. Furthermore, putaminal APT_w^{T1} MTR_{asym} correlates negatively with CFF.
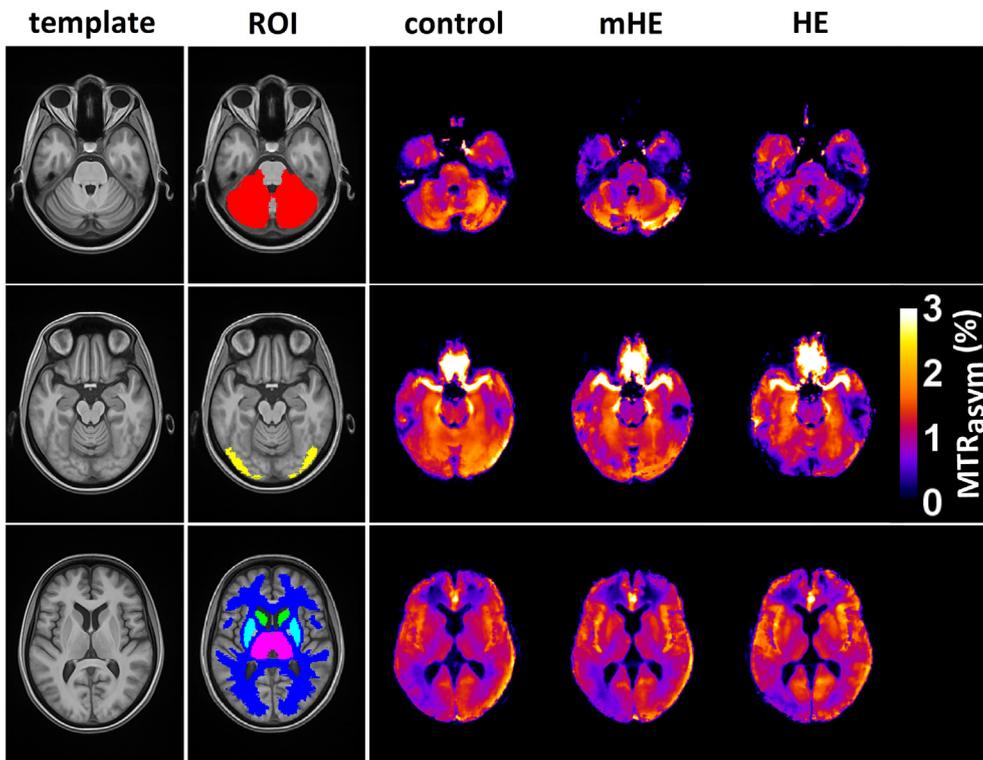
Fig. 1. Mean group atlases of APT_w MTR_{asym} in healthy controls and HE patients. The rows depict three representative slices including the six selected regions of interests (ROI) (Red: Cerebellum; Yellow: Occipital cortex; Cyan: Putamen; Magenta: Thalamus; Green: Caudate; Blue: White matter). The template of the current study population is depicted in the first column. ROI are illustrated in the second column. The last three columns display the mean atlases of the APT_w imaging of each group (control, minimal HE (mHE), manifest HE (HE)). The signal reduction could either be linked to increased ammonia accumulation or hepatocerebral degeneration.

4.1. CEST and clinical parameters in HE

Psychometric testing, CFF, and blood ammonia are common clinical parameters to assess the severity of HE, especially in cases of minimal HE, when no clinical overt signs of HE are apparent (Kircheis et al., 2014). Decreased fine motor abilities in HE patients are reflected in decreased MLS1 score, which correlate with APT_w^{T1} MTR_{asym} in the cerebellum in the present work. Increased ammonia accumulation or hepatocerebral degeneration, reflected in decreasing APT_w^{T1} MTR_{asym}, might be associated with these findings. This notion tallies previous findings demonstrating that cerebellar damage is linked to sensorimotor deficits (Miall et al., 2007) and slower upper limb movements (Manto et al., 2012). In minimal HE, motor impairments manifest in decreasing finger movement frequency and increasing movement amplitudes even prior to alterations in psychometric test scores (Butz et al., 2010). Therefore, APT_w^{T1} MTR_{asym} could shed light on cerebellar alterations leading to impaired motor performance in HE. An additional hint to this interpretation is the correlation with the motor reaction time (WRT2) score.

The contrast mechanisms behind APT_w imaging are assumed to be multifactorial and are a matter of debate in the literature today. Possible confounders are changes in pH (Zhou et al., 2003b), water content and water T1 (Lee et al., 2017), and concentration changes in metabolites and proteins (Zaiss et al., 2015), as well as altered protein conformation within intracellular protein compounds (Goerke et al., 2015), to mention a few. These factors are discussed further in 4.3. Based on our previous study and the supplementary data (Supplementary Fig. 2) we assume changes in the protein structure to be the main contributor to the observed contrast change in our study. Whether these changes are mediated through direct conformational changes in the protein structure or indirect mechanisms of ammonia, however, cannot be disentangled with the present findings. Thus, hepatocerebral degeneration (Victor et al., 1965; Yalçın et al., 2016) might contribute to the signal reduction in APT_w images in more severe HE affecting the cerebellum specifically (Butterworth, 2007). Cerebellar degeneration in HE is characterized by loss of Purkinje cells, and alcoholic abuse is associated with a greater degree of severity of loss of these cells, and a

higher HE prevalence (Kril et al., 1997). In light of the etiology of our patient cohort (50% alcoholic liver cirrhosis, 50% non-alcoholic etiology), APT_w^{T1} MTR_{asym} may be altered by an alcohol-induced high degree of cell loss in the cerebellum. Moreover, the appearance of Alzheimer type II astrocytes is likely in those patients (Kril et al., 1997). These cells undergo morphological changes and thus, might alter the APT_w^{T1} MTR_{asym} by changing the number of exchangeable amide groups within the measurement volume. Further *in vitro* CEST studies including different cell types with HE-related morphological changes might unravel their specific contribution to our findings at hand.

Previous studies reported an involvement of the visual cortex in HE. This includes worse performance in CFF tests (Kircheis et al., 2014), reduced visual GABA/Cr levels (Oeltzschner et al., 2015), abnormal neuronal activity in resting-state fMRI of the visual cortex (Chen et al., 2012), slowed frequency of of alpha and gamma band oscillations recorded with MEG (Baumgarten et al., 2018; Kahlbrock et al., 2012), and alterations in visual evoked potentials (Zeneroli et al., 1984). This involvement is reflected in significant reduction of APT_w signals within the occipital cortex and its correlation with the psychometric scores. Increased ammonia accumulation, reflected by decreasing APT_w^{T1} MTR_{asym}, could lead to an impairment of visual perception through neurotransmitter imbalance by ammonia detoxification. A link to CFF was only found within the putamen. This could be due to the fact of relatively large dispersion of the measured APT_w MTR_{asym} signals. The strong correlation of blood ammonia levels with APT_w signals in cerebellum and occipital cortex substantiates our findings as markers for HE severity.

Further liver disease related markers from the blood test, such as gamma-glutamyltransferase (GGT) concentrations displayed significant correlation with APT_w^{T1} signals in the thalamus. Future CEST studies including larger number of patients and especially patients at higher diseases stage (HE II) may help better clarifying links between clinical parameters and APT_w signals in different brain regions.

4.2. Ammonia in HE

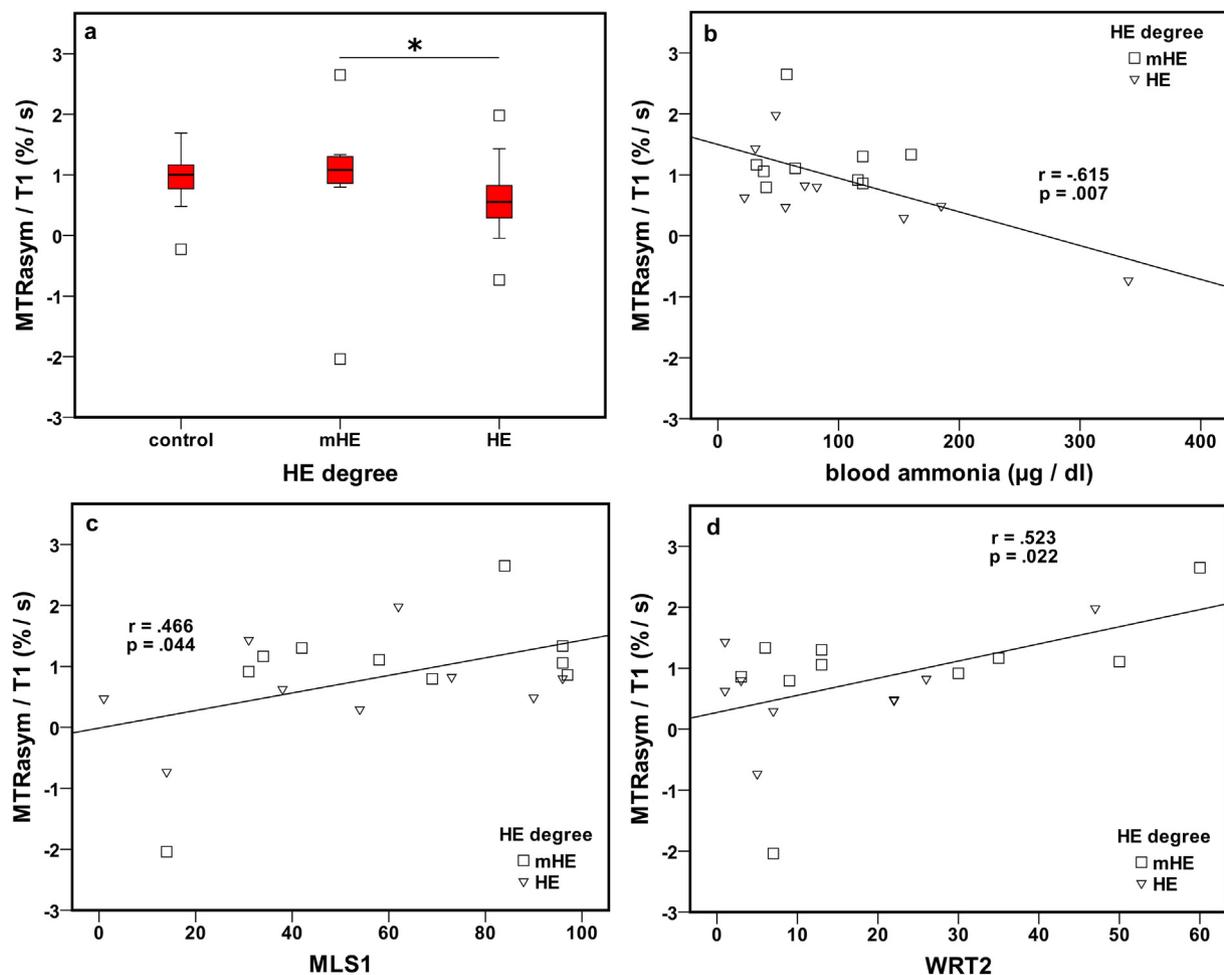The multifactorial nature of the pathophysiology of HE includes

Fig. 2. APT_w imaging of the cerebellum in healthy controls and HE patients (minimal HE (mHE), manifest HE (HE)). (a) Group boxplots including mean APT_w^{T1} MTR_{asym} values. Asterisks indicate significant differences between groups ($p < .05$). Correlations between blood ammonia levels (b), psychometric MLS1 score (hand steadiness/tremor) (c), psychometric WRT2 score (motor reaction time) (d), and mean APT_w^{T1} MTR_{asym}. The data suggests a strong cerebellar involvement in HE explaining poor motor performance of HE patients, which could possibly be linked to ammonia accumulation or hepatocerebral degeneration.

several alterations in brain metabolism, which interact with the APT_w imaging contrast. A key role in the pathophysiology is attributed to the invasion of ammonia in the patients' brains (Cichoz-Lach and Michalak, 2013; Häussinger and Sies, 2013). At physiological pH levels, ammonia remains invisible to the classical CEST approach, due to its high exchange rate. Nevertheless, our recent study could demonstrate a link between ammonia concentration and APT_w MTR_{asym} protein signal (Zöllner et al., 2018).

In vitro, the contrast mechanisms were mainly driven by an induced protein denaturation through ammonia, while contrast mechanisms remained unclear in the *in vivo* cases (Zöllner et al., 2018). Our data describes APT_w signal reductions in the cerebellum and the occipital cortex of HE patients, including correlations with blood ammonia levels and psychometric test scores. A possible interpretation is to link this reduction to an increased ammonia load in these regions, as we already assumed in our *in vitro* experiments.

Our findings are in line with an earlier $^{13}NH_3$-PET study (Keiding et al., 2006) depicting a correlation between blood ammonia and the metabolic flux of ammonia. In this work, the metabolic flux was defined as the product of the netto metabolic clearance in blood from intracellular metabolites and arterial ammonia concentration, which was deduced from radioactively marked ammonia. Intracellular glutamine is linked to ammonia removal through glutamine synthase within the brain. As APT_w signal predominantly reflects intracellular protein compounds we assume the contrast changes in our study to be mediated through ammonia within the astrocytes, which is underlined by

comparable correlations in cerebellum and cortex (Keiding et al., 2006). Therefore, we speculate APT_w signal to reflect the metabolic flux of ammonia. At present, a more elaborate differentiation of ammonia kinetic remains inaccessible with APT_w imaging as it is measured without contrast agents and reflects an averaged metabolism during the whole acquisition. In the present study, we found an increased APT_w signal in the putamen and a negative correlation with the CFF, which is in contrast to the findings reported by Keiding et al. for the basal ganglia (Keiding et al., 2006). This result indicates the potentially larger contribution of another contrast mechanism in this region. Such changes might be driven by increased manganese levels within the basal ganglia (Felipo, 2013; Häussinger and Sies, 2013; Prakash and Mullen, 2010; Rose et al., 1999; Rovira et al., 2008).

Earlier PET studies (Keiding et al., 2006; Lockwood et al., 1991) also reported increased cerebral metabolic rates and radioactivity of ammonia in the thalamus, respectively. Additionally, thalamic volume changes were found *via* voxel-based morphometry studies in HE (Lu et al., 2018). In the present study, thalamic APT_w signals only correlated with GGT concentrations. Firstly, increased glutamine concentrations could interfere with the effect of ammonia, which is complementary to our additional phantom experiments (Supplementary Fig. 2). Secondly, the changes in thalamic volume could alter the APT_w signal due to changes in the protein concentration. Thirdly, the changes in APT_w signal could be dominated by hepatocerebral degeneration, which possibly differs between various regions. Yet, these explanations need to remain speculative.
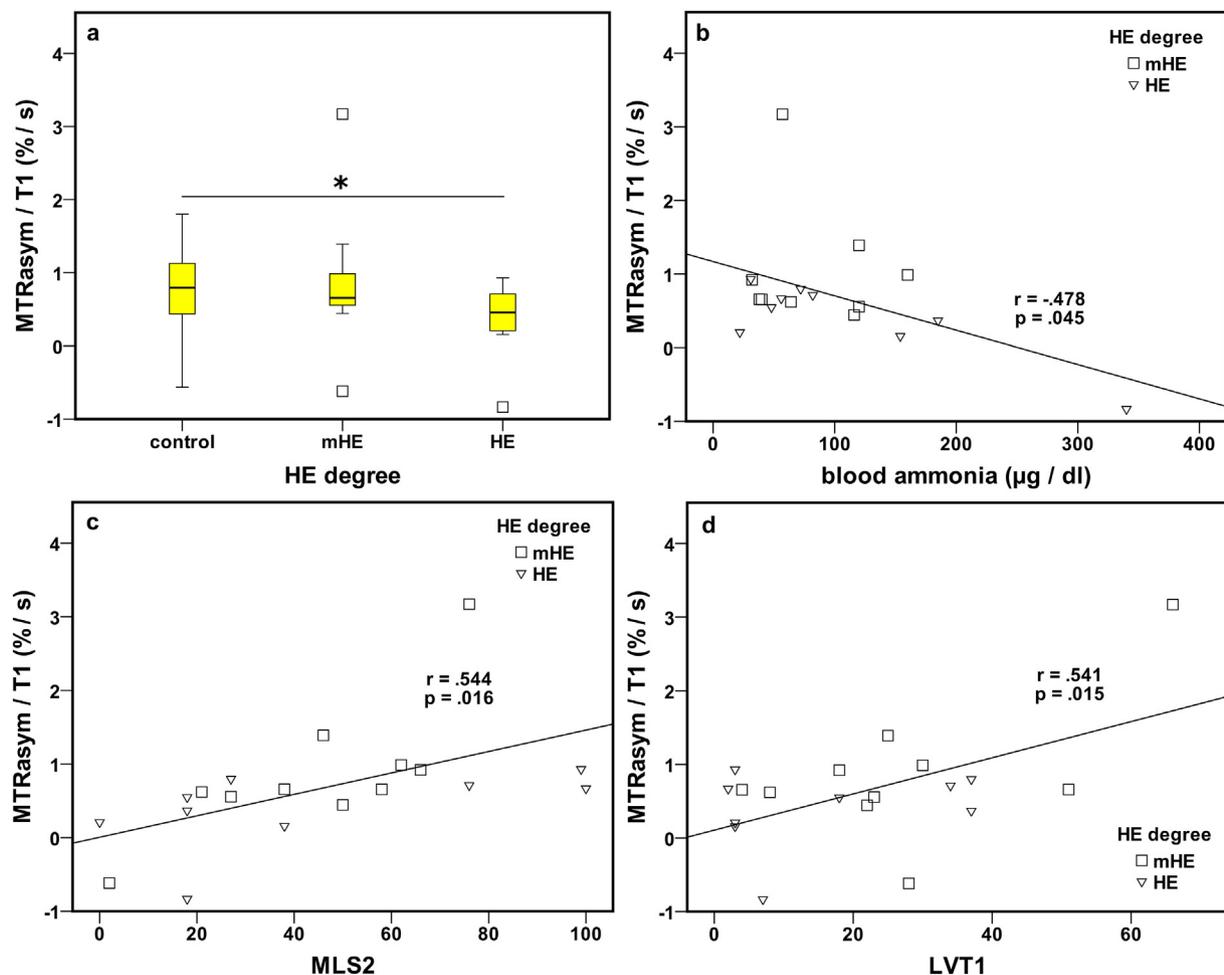
Fig. 3. APT_w imaging of the occipital cortex in healthy controls and HE patients (minimal HE (mHE), manifest HE (HE)). (a) Group boxplots including mean APT_w^{T1} MTR_{asym} values. Asterisks indicate significant differences between groups ($p < .05$). Correlations between blood ammonia levels (b), psychometric MLS2 score (arm/hand precision) (c), psychometric LVT1 score (time per item) (d), and mean APT_w^{T1} MTR_{asym} values. This might explain alterations in visual perception of HE patients with increasing diseases severity due to ammonia accumulation.

Ammonia detoxification by glutamine synthase triggers the accumulation of glutamine within astrocytes (Felipo, 2013; Häussinger and Sies, 2013; Prakash and Mullen, 2010). Several studies reported disturbance in glutamate/glutamine balance, such as increasing glutamine concentrations after chronic liver failure in rat models (Swain et al., 1992), and elevated glutamine concentrations in basal ganglia (Miese et al., 2006) and cortical brain regions of HE patients (Häussinger et al., 1994; Kreis et al., 1991; Oeltzschner et al., 2015). Glutamine and glutamate are both CEST-sensitive, and resonate between 3 and 4 ppm (Schmidt et al., 2016).

As a result, signal contributions of both metabolites might interact with the APT_w mechanism used in this study. In this case, the increasing APT_w signal and the negative correlation with the CFF in the putamen could be interpreted as increased glutamate + glutamine (Glx) ratios. In additional phantom experiments (Supplementary Fig. 2), we found that ammonia dominates the contrast mechanism with its presence, by adding *in vivo* realistic glutamate, glutamine (control and HE concentrations), and ammonia concentrations in one solution.

Besides, a 3 T system does not have a high sensitivity to depict changes in either glutamate or glutamine (Lee et al., 2016), but showed sensitivity to ammonia load in protein based solutions (Zöllner et al., 2018). Hence, the underlying mechanisms in the putamen remain unclear, but are likely to be linked to HE disease severity.

4.3. CEST-sensitive confounders

Starting from APT_w imaging, we adapted our saturation parameters in two ways (Zöllner et al., 2018). In *in vitro* experiments, the saturation parameters were selected to maximize the contrast gained from the effect of ammonia on the protein signal. Then, these saturation parameters were used to create full brain coverage within the *in vivo* measurements. *In vitro,* we were able to link the alterations in APT_w signals directly to ammonia, but *in vivo,* ammonia could only be one of a few contributors to the alterations. Another physiological change described for HE is the osmotic imbalance, which is triggered through the ammonia depletion. Finally, alterations in brain water homeostasis and the emergence of a low-grade edema are reported (Häussinger and Schliess, 2008). Regarding the MR visibility of these changes, one study reported water content changes of about 2% in several brain regions including the putamen (Shah et al., 2008), whereas an absence of MR visible water content changes was reported in another study in HE patients in less severe stages (Oeltzschner et al., 2016).

Several APT_w CEST studies at 4.7 T and 7 T emphasize that water content plays a minor role in the contrast formation of APT only (Khlebnikov et al., 2016; Lee et al., 2017). However, as the APT_w values were normalized by the T1 relaxation time, any possible T1 effect can be neglected.

Quantitative T_1 (Shah et al., 2003) and T_1-weighted (Butterworth et al., 1995; Klos et al., 2006; Pujol et al., 1993; Rovira et al., 2008)

mechanisms. In addition, a recent study claimed that MTR_{asym} of amide protons at the saturation parameters (B_1, t_{sat}) used in the present study is roughly insensitive to water longitudinal relaxation time (Zu, 2018).

4.4. Limitations

One limitation of the present study is the number of included patients. As our data suggests that the APT_w signals are strongly altered in manifest HE, the inclusion of more patients in the higher HE grade could have strengthened our findings. However, the inclusion of patients in higher disease stages is hard to achieve, as patient compliance is needed both to perform psychometric testing and to achieve sufficient quality of MR data without a substantial amount of movement artifacts.

Another limitation is the number of analyzed ROIs, which included prior knowledge and assumptions within the analysis and led to the fact that some effects might be missed in other brain regions. Thus, all interpretations remain descriptive in the first place and final conclusions about affected brain regions and APT_w imaging as marker for HE severity have to be confirmed in future larger studies. In addition, the inclusion of larger cohorts would allow the implementation of nonparametric voxel based analysis (Holmes et al., 1996). This technique excludes user-biased ROI analysis and could give further insight in the disease progression and spatial distribution of HE-related changes. Nevertheless, the present study indicates that APT_w imaging is a possible marker for HE, as correlations with HE-related clinical markers were evident.

The sensitivity of the CEST technique is another limitation and a possible explanation for the absence of thalamic alterations in the present study. As discussed above, several confounders to the APT_w signal remain elusive, which could lead to increasing type II error rates. In future studies, a combination of MRS with the CEST technique could shed light on the underlying contrast mechanisms. By using the voxel-based acquisition technique EXPRESS (Walker-Samuel et al., 2012) in combination with J-difference-edited MEGA-PRESS spectroscopy (Mescher et al., 1998) or a novel accelerated spectral editing sequence allowing the measurement of multiple compounds at the same time in the same brain region (Saleh et al., 2016), the interplay between neurotransmitter metabolism (GABA, glutamate, glutamine), osmolytes (myo-inositol), oxidative stress markers (glutathione), and changes in the protein signals could be investigated. These studies may focus on alterations in cerebellum and thalamus, as the interplay of metabolism and HE is yet unclear in these regions. Additional acquisition of water references would further allow drawing conclusions about water content.

To reach sufficient acquisition times and full brain coverage, relatively short saturation times, small numbers of saturation frequencies,
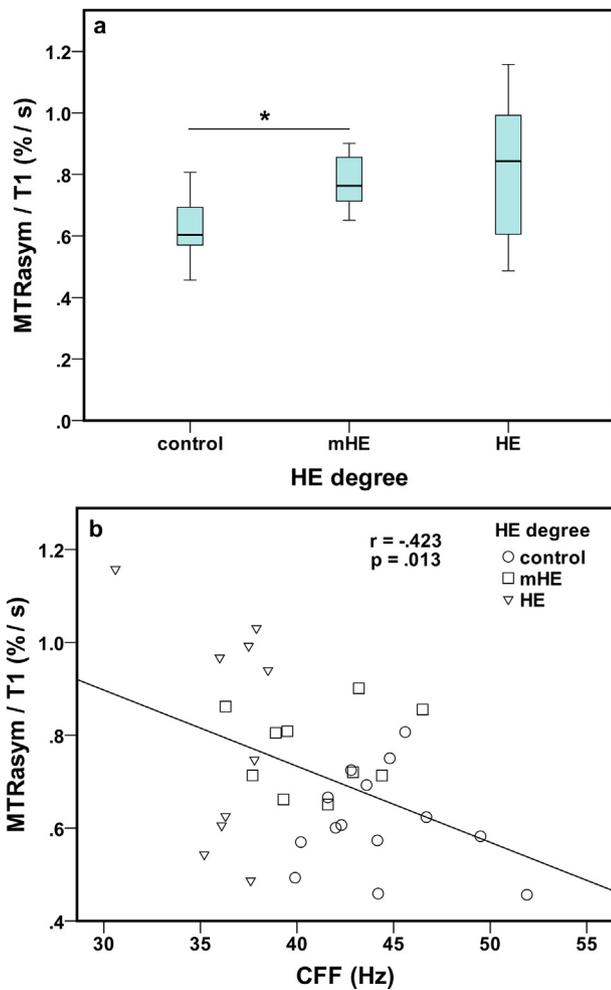
Fig. 4. APT_w imaging of the putamen in healthy controls and HE patients (minimal HE (mHE), manifest HE (HE)). (a) Group boxplots including mean APT_w^{T1} MTR_{asym}. Asterisks indicate significant differences between groups (p < .05). (b) Correlation between critical flicker frequency (CFF) and mean APT_w^{T1} MTR_{asym} values. The data suggests the domination of other contrast mechanisms, such as metabolite concertation changes.

changes are known to be a key finding in MR imaging of hepatic encephalopathy. To rule out the contamination of our MTR_{asym} we employed a T_1 normalization, which resolves in pure APT_w contrast

Table 3
Correlations of psychometric test scores and mean APT_w^{T1} MTR_{asym} (COG1: time to reject a geometric shape not matching control shapes; COG2: time to confirm a geometric shape matching a control shape; line following: LVT1: time per item; LVT2: overall score; MLS1: hand steadiness/tremor; MLS2: arm/hand precision; MLS3: arm/hand speed; MLS4: finger tapping speed; WRT1: reaction time; WRT2: motor reaction time). Bold numbers indicate significant correlations.

	COG1	COG2	LVT1	LVT2	MLS1	MLS2	MLS3	MLS4	WRT1	WRT2
	r	r	r	r	r	r	r	r	r	r
	p	p	p	p	p	p	p	p	p	p
Cerebellum	0.164	0.162	0.299	0.277	**0.466**	0.443	0.357	0.156	0.282	**0.523**
	0.503	0.508	0.213	0.250	**0.044**	0.058	0.133	0.525	0.243	**0.022**
Occipital cortex	0.378	0.400	**0.547**	**0.469**	0.399	**0.544**	**0.526**	−0.092	0.356	**0.531**
	0.110	0.089	**0.015**	**0.043**	0.091	**0.016**	**0.021**	0.708	0.019	**0.019**
Putamen	−0.093	−0.105	0.318	0.391	0.314	−0.034	−0.013	0.258	−0.139	0.285
	0.704	0.668	0.184	0.098	0.191	0.890	0.958	0.286	0.569	0.237
Thalamus	−0.070	−0.102	0.124	0.185	0.181	0.272	0.181	0.038	−0.056	0.188
	0.776	0.678	0.614	0.449	0.458	0.260	0.458	0.876	0.821	0.441
Caudate	−0.335	−0.381	−0.150	−0.146	0.151	−0.174	−0.301	0.384	−0.373	0.005
	0.161	0.108	0.539	0.552	0.538	0.476	0.210	0.104	0.116	0.985
White matter	−0.140	−0.170	0.038	0.114	0.236	0.356	0.108	−0.021	0.002	0.099
	0.567	0.488	0.876	0.643	0.330	0.135	0.659	0.930	0.994	0.688

and a non-steady state acquisition were chosen in the present study. Faster imaging sequences would allow improving those parameters, which could even include steady-state CEST measurements within the acquisition. As a result, further correction of the CEST signal could be implemented, such as AREX (Zaiss et al., 2015) or EMR (Heo et al., 2016). More advanced quantification approaches like Lorentzian fitting (Zaiss et al., 2011) could also improve data quality and strengthen the findings. Additionally, a Lorentzian fitting model could be able to distinguish between APT, Nuclear Overhauser effect (NOE), and MTC, if a suitable model is chosen. Apart from the fact that ammonia only affects the APT exchange in *in vitro* experiments (Zöllner et al., 2018), some *in vivo* studies reported MTC to be altered in HE patients (Miese et al., 2006). Moreover, morphological changes might affect the NOE, thus Lorentzian fitting could give further insight to the underlying contrast mechanisms in HE. It was not implemented in the current study, as it requires a large number of saturation frequencies leading to long total acquisition times. The implemented MTR_{asym} analysis combined with the full brain coverage already permits the distinction between controls and patients, based on APT_w signal alterations in several brain regions.

5. Conclusions

Hepatic encephalopathy is associated with a region-specific decrease of APT_w signals, in particularly in the cerebellum and the occipital cortex. These signal changes are linked to increased blood ammonia concentrations, and clinical scores of cognitive and motor function. These variations are most likely a consequence of hyperammonemia or hepatocerebral degeneration processes and develop in parallel with disease severity. Therefore, APT_w CEST imaging could be a possible tool to investigate HE and advance the understanding of region-specific alterations in HE and its clinical equivalents. By including additional methods to quantify metabolite levels and water content, the interplay between metabolism and protein signal alterations in HE could be assessed in more detail in future studies.

Conflict of interest

D.H. belongs to a group of patent holders for the bedside measurement device determining the critical flicker frequency.

Appendix A. Supplementary data

Supplementary data to this article can be found online at https://doi.org/10.1016/j.nicl.2019.101743.

References

Avants, B.B., Tustison, N.J., Song, G., Gee, J.C., 2009. ANTS: Advanced Open-Source Normalization Tools for Neuroanatomy. Penn IMage Computing and Science Laboratory.

Avants, B.B., Tustison, N.J., Song, G., Cook, P.A., Klein, A., Gee, J.C., 2011. A reproducible evaluation of ANTs similarity metric performance in brain image registration. Neuroimage 54, 2033–2044. https://doi.org/10.1016/j.neuroimage.2010.09.025.

Baumgarten, T.J., Neugebauer, J., Oeltzschner, G., Füllenbach, N.D., Kircheis, G., Häussinger, D., Lange, J., Wittsack, H.J., Butz, M., Schnitzler, A., 2018. Connecting occipital alpha band peak frequency, visual temporal resolution, and occipital GABA levels in healthy participants and hepatic encephalopathy patients. NeuroImage Clin. 20, 347–356. https://doi.org/10.1016/j.nicl.2018.08.013.

Butterworth, R.F., 2000. Complications of cirrhosis III. Hepatic encephalopathy. J. Hepatol. 32, 171–180. https://doi.org/10.1016/S0168-8278(00)80424-9.

Butterworth, R.F., 2007. Neuronal cell death in hepatic encephalopathy. Metab. Brain Dis. 22, 309–320. https://doi.org/10.1007/s11011-007-9072-3.

Butterworth, R.F., Spahr, L., Fontaine, S., Layrargues, G.P., 1995. Manganese toxicity, dopaminergic dysfunction and hepatic encephalopathy. Metab. Brain Dis. 10, 259–267. https://doi.org/10.1007/BF02109357.

Butz, M., Timmermann, L., Braun, M., Groiss, S.J., Wojtecki, L., Ostrowski, S., Krause, H., Pollok, B., Gross, J., Südmeyer, M., Kircheis, G., Häussinger, D., Schnitzler, A., 2010. Motor impairment in liver cirrhosis without and with minimal hepatic encephalopathy. Acta Neurol. Scand. 122, 27–35. https://doi.org/10.1111/j.1600-0404.2009.01246.x.

Cauli, O., Rodrigo, R., Llansola, M., Montoliu, C., Monfort, P., Piedrafita, B., El Mlili, N., Boix, J., Agustí, A., Felipo, V., 2009. Glutamatergic and gabaergic neurotransmission and neuronal circuits in hepatic encephalopathy. Metab. Brain Dis. 24, 69–80. https://doi.org/10.1007/s11011-008-9115-4.

Chen, H.J., Zhu, X.Q., Jiao, Y., Li, P.C., Wang, Y., Teng, G.J., 2012. Abnormal baseline brain activity in low-grade hepatic encephalopathy: a resting-state fMRI study. J. Neurol. Sci. 318, 140–145. https://doi.org/10.1016/j.jns.2012.02.019.

Cichoz-Lach, H., Michalak, A., 2013. Current pathogenetic aspects of hepatic encephalopathy and noncirrhotic hyperammonemic encephalopathy. World J. Gastroenterol. https://doi.org/10.3748/wjg.v19.i1.26.

Detry, O., De Roover, A., Honoré, P., Meurisse, M., 2006. Brain edema and intracranial hypertension in fulminant hepatic failure: pathophysiology and management. World J. Gastroenterol. 12, 7405–7412. https://doi.org/10.3748/wjg.v12.i46.7405.

Felipo, V., 2013. Hepatic encephalopathy: effects of liver failure on brain function. Nat. Rev. Neurosci. 14, 851–858. https://doi.org/10.1038/nrn3587.

Ferenci, P., Blei, A.T., Lockwood, A.H., Mullen, K., Tarter, R., Weissenborn, K., 2002. Hepatic encephalopathy - definition, nomenclature, diagnosis, and quantification: final report of the working party at the 11th world congresses of gastroenterology, Vienna, 1998. Hepatology 35, 716–721. https://doi.org/10.1053/jhep.2002.31250.

Friston, K., 2007. Statistical Parametric Mapping: The Analysis of Functional Brain Images. Academic Press.

Goerke, S., Zaiss, M., Kunz, P., Klika, K.D., Windschuh, J.D., Mogk, A., Bukau, B., Ladd, M.E., Bachert, P., 2015. Signature of protein unfolding in chemical exchange saturation transfer imaging. NMR Biomed. 28, 906–913. https://doi.org/10.1002/nbm.3317.

Goerke, S., Milde, K.S., Bukowiecki, R., Kunz, P., Klika, K.D., Wiglenda, T., Mogk, A., Wanker, E.E., Bukau, B., Ladd, M.E., Bachert, P., Zaiss, M., 2017. Aggregation-induced changes in the chemical exchange saturation transfer (CEST) signals of proteins. NMR Biomed. 30. https://doi.org/10.1002/nbm.3665.

Häussinger, D., Schliess, F., 2008. Pathogenetic mechanisms of hepatic encephalopathy. Gut 57, 1156–1165. https://doi.org/10.1136/gut.2007.122176.

Häussinger, D., Sies, H., 2013. Editorial: hepatic encephalopathy: clinical aspects and pathogenetic concept. Arch. Biochem. Biophys. 536, 97–100. https://doi.org/10.1016/j.abb.2013.04.013.

Häussinger, D., Laubenberger, J., Vom Dahl, S., Ernst, T., Bayer, S., Langer, M., Gerok, W., Hennig, J., 1994. Proton magnetic resonance spectroscopy studies on human brain Myo-inositol in hypo-osmolarity and hepatic encephalopathy. Gastroenterology 107, 1475–1480. https://doi.org/10.1016/0016-5085(94)90552-5.

Heo, H.-Y., Zhang, Y., Jiang, S., Lee, D.-H., Zhou, J., 2016. Quantitative assessment of amide proton transfer (APT) and nuclear overhauser enhancement (NOE) imaging with extrapolated semisolid magnetization transfer reference (EMR) signals: II. Comparison of three EMR models and application to human brain glioma at 3 Tesla. Magn. Reson. Med. 75, 1630–1639. https://doi.org/10.1002/mrm.25795.

Holmes, A.P., Blair, R.C., Watson, J.D.G., Ford, I., 1996. Nonparametric analysis of statistic images from functional mapping experiments. J. Cereb. Blood Flow Metab. 16, 7–22. https://doi.org/10.1097/00004647-199601000-00002.

Jones, C.K., Polders, D., Hua, J., Zhu, H., Hoogduin, H.J., Zhou, J., Luijten, P.R., van Zijl, P.C.M., 2012. In vivo three-dimensional whole-brain pulsed steady-state chemical exchange saturation transfer at 7 T. Magn. Reson. Med. 67, 1579–1589. https://doi.org/10.1002/mrm.23141.

Kahlbrock, N., Butz, M., May, E.S., Brenner, M., Kircheis, G., Häussinger, D., Schnitzler, A., 2012. Lowered frequency and impaired modulation of gamma band oscillations in a bimodal attention task are associated with reduced critical flicker frequency. Neuroimage 61, 216–227. https://doi.org/10.1016/j.neuroimage.2012.02.063.

Keiding, S., Sørensen, M., Bender, D., Munk, O.L., Ott, P., Vilstrup, H., 2006. Brain metabolism of 13N-ammonia during acute hepatic encephalopathy in cirrhosis measured by positron emission tomography. Hepatology 43, 42–50. https://doi.org/10.1002/hep.21001.

Khlebnikov, V., Siero, J.C.W., Wijnen, J.P., Visser, F., Luijten, P.R., Klomp, D.W.J., Hoogduin, H.J., 2016. Is there any difference in Amide and NOE CEST effects between white and gray matter at 7 T? J. Magn. Reson. 272, 82–86. https://doi.org/10.1016/j.jmr.2016.09.010.

Kim, M., Gillen, J., Landman, B.A., Zhou, J., van Zijl, P.C.M., 2009. Water saturation shift referencing (WASSR) for chemical exchange saturation transfer (CEST) experiments. Magn. Reson. Med. 61, 1441–1450. https://doi.org/10.1002/mrm.21873.

Kircheis, G., Häussinger, D., Wettstein, M., Schnitzler, A., Timmermann, L., 2002. Critical flicker frequency for quantification of low-grade hepatic encephalopathy. Hepatology 35, 357–366. https://doi.org/10.1053/jhep.2002.30957.

Kircheis, G., Hilger, N., Häussinger, D., 2014. Value of Critical Flicker Frequency and psychometric hepatic encephalopathy score in diagnosis of low-grade hepatic encephalopathy. Gastroenterology 146, 961–969. e11. https://doi.org/10.1053/j.gastro.2013.12.026.

Klos, K.J., Ahlskog, J.E., Kumar, N., Cambern, S., Butz, J., Burritt, M., Fealey, R.D., Cowl, C.T., Parisi, J.E., Josephs, K.A., 2006. Brain metal concentrations in chronic liver failure patients with pallidal T1 MRI hyperintensity. Neurology 67, 1984–1989. https://doi.org/10.1212/01.wnl.0000247037.37807.76.

Kreis, R., Farrow, N., Ross, B.D., 1991. Localized 1H NMR spectroscopy in patients with chronic hepatic encephalopathy. Analysis of changes in cerebral glutamine, choline and inositols. NMR Biomed. 4, 109–116. https://doi.org/10.1002/nbm.1940040214.

Kril, J.J., Flowers, D., Butterworth, R.F., 1997. Distinctive pattern of bergmann glial pathology in human hepatic encephalopathy. Mol. Chem. Neuropathol. 31, 279–287. https://doi.org/10.1007/BF02815130.

Lee, J.S., Xia, D., Jerschow, A., Regatte, R.R., 2016. In vitro study of endogenous CEST agents at 3T and 7T. Contrast Media Mol. Imaging 11, 4–14. https://doi.org/10.1002/cmmi.1652.

Lee, D.-H., Heo, H.-Y., Zhang, K., Zhang, Y., Jiang, S., Zhao, X., Zhou, J., 2017. Quantitative assessment of the effects of water proton concentration and water T_1 changes on amide proton transfer (APT) and nuclear overhauser enhancement (NOE) MRI: the origin of the APT imaging signal in brain tumor. Magn. Reson. Med. 77, 855–863. https://doi.org/10.1002/mrm.26131.

Lockwood, A.H., Yap, E.W.H., Wong, W.-H., 1991. Cerebral ammonia metabolism in patients with severe liver disease and minimal hepatic encephalopathy. J. Cereb. Blood Flow Metab. 11, 337–341. https://doi.org/10.1038/jcbfm.1991.67.

Lu, C.-Q., Jiao, Y., Meng, X.-P., Cai, Y., Luan, Y., Xu, X.-M., Ju, S., 2018. Structural change of thalamus in cirrhotic patients with or without minimal hepatic encephalopathy and the relationship between thalamus volume and clinical indexes related to cirrhosis. NeuroImage Clin. https://doi.org/10.1016/j.NICL.2018.09.015.

Manjón, J.V., Carbonell-Caballero, J., Lull, J.J., García-Martí, G., Martí-Bonmatí, L., Robles, M., 2008. MRI denoising using non-local means. Med. Image Anal. 12, 514–523. https://doi.org/10.1016/j.media.2008.02.004.

Manto, M., Bower, J.M., Conforto, A.B., Delgado-García, J.M., Da Guarda, S.N.F., Gerwig, M., Habas, C., Hagura, N., Ivry, R.B., Marien, P., Molinari, M., Naito, E., Nowak, D.A., Ben Taib, N.O., Pelisson, D., Tesche, C.D., Tilikete, C., Timmann, D., 2012. Consensus paper: roles of the cerebellum in motor control-the diversity of ideas on cerebellar involvement in movement. Cerebellum 11, 457–487. https://doi.org/10.1007/s12311-011-0331-9.

Mescher, M., Merkle, H., Kirsch, J., Garwood, M., Gruetter, R., 1998. Simultaneous in vivo spectral editing and water suppression. NMR Biomed. 11, 266–272. https://doi.org/10.1002/(SICI)1099-1492(199810)11:6<266::AID-NBM530>3.0.CO;2-J.

Miall, R.C., Christensen, L.O.D., Cain, O., Stanley, J., 2007. Disruption of state estimation in the human lateral cerebellum. PLoS Biol. 5, e316. https://doi.org/10.1371/journal.pbio.0050316.

Miese, F., Kircheis, G., Wittsack, H.-J., Wenserski, F., Hemker, J., Mödder, U., Häussinger, D., Cohnen, M., 2006. 1H-MR spectroscopy, magnetization transfer, and diffusion-weighted imaging in alcoholic and nonalcoholic patients with cirrhosis with hepatic encephalopathy. Am. J. Neuroradiol. 27, 1019–1026 (doi:27/5/1019 [pii]).

Mori, S., Eleff, S.M., Pilatus, U., Mori, N., van Zijl, P.C.M., 1998. Proton NMR spectroscopy of solvent-saturable resonances: a new approach to study pH effects in situ. Magn. Reson. Med. 40, 36–42. https://doi.org/10.1002/mrm.1910400105.

Norenberg, M.D., Rama Rao, K.V., Jayakumar, A.R., 2005. Mechanisms of ammonia-induced astrocyte swelling. Metab. Brain Dis. 20, 303–318. https://doi.org/10.1007/s11011-005-7911-7.

Oeltzschner, G., Butz, M., Baumgarten, T.J., Hoogenboom, N., Wittsack, H.-J., Schnitzler, A., 2015. Low visual cortex GABA levels in hepatic encephalopathy: links to blood ammonia, critical flicker frequency, and brain osmolytes. Metab. Brain Dis. 30, 1429–1438. https://doi.org/10.1007/s11011-015-9729-2.

Oeltzschner, G., Butz, M., Wickrath, F., Wittsack, H.-J., Schnitzler, A., 2016. Covert hepatic encephalopathy: elevated total glutathione and absence of brain water content changes. Metab. Brain Dis. 31, 517–527. https://doi.org/10.1007/s11011-015-9760-3.

Prakash, R., Mullen, K.D., 2010. Mechanisms, diagnosis and management of hepatic encephalopathy. Nat. Rev. Gastroenterol. Hepatol. 7, 515–525. https://doi.org/10.1038/nrgastro.2010.116.

Pujol, A., Pujol, J., Graus, F., Rimola, A., Peri, J., Mercader, J.M., Garcia-Pagan, J.C., Bosch, J., Rodes, J., Tolosa, E., 1993. Hyperintense globus pallidus on T1-weighted MRI in cirrhotic patients is associated with severity of liver failure. Neurology 43, 65. https://doi.org/10.1212/WNL.43.1_Part_1.65.

Rose, C., Butterworth, R.F., Zayed, J., Normandin, L., Todd, K., Michalak, A., Spahr, L., Huet, P.M., Pomier-Layrargues, G., 1999. Manganese deposition in basal ganglia structures results from both portal-systemic shunting and liver dysfunction. Gastroenterology 117, 640–644. https://doi.org/10.1016/S0016-5085(99)70457-9.

Rovira, A., Alonso, J., Córdoba, J., 2008. MR imaging findings in hepatic encephalopathy. Am. J. Neuroradiol. 29, 1612–1621. https://doi.org/10.3174/ajnr.A1139.

Sabati, M., Maudsley, A.A., 2013. Fast and high-resolution quantitative mapping of tissue water content with full brain coverage for clinically-driven studies. Magn. Reson. Imaging 31, 1752–1759. https://doi.org/10.1016/j.mri.2013.08.001.

Saleh, M.G., Oeltzschner, G., Chan, K.L., Puts, N.A.J., Mikkelsen, M., Schär, M., Harris, A.D., Edden, R.A.E., 2016. Simultaneous edited MRS of GABA and glutathione. Neuroimage 142, 576–582. https://doi.org/10.1016/j.neuroimage.2016.07.056.

Schmidt, H., Schwenzer, N.F., Gatidis, S., Küstner, T., Nikolaou, K., Schick, F., Martirosian, P., 2016. Systematic evaluation of amide proton chemical exchange saturation transfer at 3 T. Investig. Radiol. 51, 635–646. https://doi.org/10.1097/RLI.0000000000000292.

Shah, N.J., Neeb, H., Zaitsev, M., Steinhoff, S., Kircheis, G., Amunts, K., Häussinger, D., Zilles, K., 2003. Quantitative T1Mapping of hepatic encephalopathy using magnetic resonance imaging. Hepatology 38, 1219–1226. https://doi.org/10.1053/jhep.2003.50477.

Shah, N.J., Neeb, H., Kircheis, G., Engels, P., Häussinger, D., Zilles, K., 2008. Quantitative cerebral water content mapping in hepatic encephalopathy. Neuroimage 41, 706–717. https://doi.org/10.1016/j.neuroimage.2008.02.057.

Swain, M., Butterworth, R.F., Blei, A.T., 1992. Ammonia and related amino acids in the pathogenesis of brain edema in acute ischemic liver failure in rats. Hepatology 15, 449–453. https://doi.org/10.1002/hep.1840150316.

van Zijl, P.C.M., Zhou, J., Mori, N., Payen, J.F., Wilson, D.A., Mori, S., 2003. Mechanism of magnetization transfer during on-resonance water saturation. A new approach to detect mobile proteins, peptides, and lipids. Magn. Reson. Med. 49, 440–449. https://doi.org/10.1002/mrm.10398.

Victor, M., Adams, R.D., Cole, M., 1965. The acquired (non-wilsonian) type of chronic hepatocerebral degeneration. Med. (United States) 44, 345–396. https://doi.org/10.1097/00005792-196509000-00001.

Walker-Samuel, S., Johnson, S.P., Pedley, B., Lythgoe, M.F., Golay, X., 2012. Extracranial measurements of amide proton transfer using exchange-modulated point-resolved spectroscopy (EXPRESS). NMR Biomed. 25, 829–834. https://doi.org/10.1002/nbm.1798.

Windschuh, J.D., Zaiss, M., Meissner, J.E., Paech, D., Radbruch, A., Ladd, M.E., Bachert, P., 2015. Correction of B1-inhomogeneities for relaxation-compensated CEST imaging at 7T. NMR Biomed. 28, 529–537. https://doi.org/10.1002/nbm.3283.

Wolff, S.D., Balaban, R.S., 1989. Magnetization transfer contrast (MTC) and tissue water proton relaxation in vivo. Magn. Reson. Med. 10, 135–144. https://doi.org/10.1002/mrm.1910100113.

World Medical Association declaration of Helsinki: Ethical principles for medical research involving human subjects, 2013. J. Am. Med. Assoc. 310, 2191–2194. https://doi.org/10.1001/jama.2013.281053.

Yalçın, A.D., Oğuz-Akarsu, E., Sökmen, H.M., 2016. Acquired hepatocerebral degeneration. Neurosciences 21, 164–167. https://doi.org/10.17712/nsj.2016.2.20150164.

Yuan, J., Mok, G.S.P., Zhang, Q., Wang, Y.-X., Zhou, J., 2016. Improved quantification of chemical exchange saturation transfer (CEST) MRI using nonlocal means. In: 2014 IEEE Nuclear Science Symposium and Medical Imaging Conference, NSS/MIC 2014. IEEE, pp. 1–5. https://doi.org/10.1109/NSSMIC.2014.7430844.

Zaiss, M., Schmitt, B., Bachert, P., 2011. Quantitative separation of CEST effect from magnetization transfer and spillover effects by Lorentzian-line-fit analysis of z-spectra. J. Magn. Reson. 211, 149–155. https://doi.org/10.1016/j.jmr.2011.05.001.

Zaiss, M., Windschuh, J.D., Paech, D., Meissner, J.E., Burth, S., Schmitt, B., Kickingereder, P., Wiestler, B., Wick, W., Bendszus, M., Schlemmer, H.P., Ladd, M.E., Bachert, P., Radbruch, A., 2015. Relaxation-compensated CEST-MRI of the human brain at 7T: unbiased insight into NOE and amide signal changes in human glioblastoma. Neuroimage 112, 180–188. https://doi.org/10.1016/j.neuroimage.2015.02.040.

Zeneroli, M.L., Pinelli, G., Gollini, G., Penne, A., Messori, E., Zani, G., Ventura, E., 1984. Visual evoked potential: a diagnostic tool for the assessment of hepatic encephalopathy. Gut 25, 291–299. https://doi.org/10.1136/gut.25.3.291.

Zhang, Y., Heo, H.-Y., Lee, D.-H., Zhao, X., Jiang, S., Zhang, K., Li, H., Zhou, J., 2016. Selecting the reference image for registration of CEST series. J. Magn. Reson. Imaging 43, 756–761. https://doi.org/10.1002/jmri.25027.

Zhou, J., van Zijl, P.C.M., 2006. Chemical exchange saturation transfer imaging and spectroscopy. Prog. Nucl. Magn. Reson. Spectrosc. 48, 109–136. https://doi.org/10.1016/j.pnmrs.2006.01.001.

Zhou, J., Lal, B., Wilson, D.A., Laterra, J., van Zijl, P.C.M., 2003a. Amide proton transfer (APT) contrast for imaging of brain tumors. Magn. Reson. Med. 50, 1120–1126. https://doi.org/10.1002/mrm.10651.

Zhou, J., Payen, J.F., Wilson, D.A., Traystman, R.J., van Zijl, P.C.M., 2003b. Using the amide proton signals of intracellular proteins and peptides to detect pH effects in MRI. Nat. Med. 9, 1085–1090. https://doi.org/10.1038/nm907.

Zhou, I.Y., Lu, D., Ji, Y., Wu, L., Wang, E., Cheung, J., Zhang, X.A., Sun, P.Z., 2018. Determination of multipool contributions to endogenous amide proton transfer effects in global ischemia with high spectral resolution in vivo chemical exchange saturation transfer MRI. Magn. Reson. Med. 81, 645–652. https://doi.org/10.1002/mrm.27385.

Zöllner, H.J., Butz, M., Kircheis, G., Klinker, S., Häussinger, D., Schmitt, B., Schnitzler, A., Wittsack, H.-J., 2018. Ammonia-weighted imaging by chemical exchange saturation transfer MRI at 3 T. NMR Biomed. e3947. https://doi.org/10.1002/nbm.3947.

Zu, Z., 2018. Towards the complex dependence of MTR_{asym} on T_{1w} in amide proton transfer (APT) imaging. NMR Biomed. 31, e3934. https://doi.org/10.1002/nbm.3934.